



# HHS Public Access

Author manuscript

*Eur Radiol.* Author manuscript; available in PMC 2020 April 01.

Published in final edited form as:

*Eur Radiol.* 2019 April ; 29(4): 2017–2026. doi:10.1007/s00330-018-5735-1.

## Quantitative Susceptibility Mapping in the Human Fetus to Measure Blood Oxygenation in the Superior Sagittal Sinus

Brijesh Kumar Yadav<sup>1,2</sup>, Sagar Buch<sup>3</sup>, Uday Krishnamurthy<sup>1,2</sup>, Pavan Jella<sup>1</sup>, Edgar Hernandez-Andrade<sup>4,5</sup>, Anabela Trifan<sup>1</sup>, Lami Yeo<sup>4,5</sup>, Sonia S. Hassan<sup>4,5,6</sup>, E. Mark Haacke<sup>1,2</sup>, Roberto Romero<sup>4,7,8,9,\*</sup>, and Jaladhar Neelavalli<sup>1,10,\*</sup>

<sup>1</sup>Department of Radiology, Wayne State University School of Medicine, Detroit, Michigan, USA

<sup>2</sup>Department of Biomedical Engineering, Wayne State University College of Engineering, Detroit, Michigan, USA

<sup>3</sup>The MRI Institute for Biomedical Research, Waterloo, Ontario, Canada

<sup>4</sup>Perinatology Research Branch, NICHD/NIH/DHHS, Bethesda, Maryland, and Detroit, Michigan, USA

<sup>5</sup>Department of Obstetrics and Gynecology, Wayne State University School of Medicine, Detroit, Michigan, USA

<sup>6</sup>Department of Physiology, Wayne State University School of Medicine, Detroit, Michigan, USA

<sup>7</sup>Department of Obstetrics and Gynecology, University of Michigan, Ann Arbor, Michigan, USA

<sup>8</sup>Department of Epidemiology and Biostatistics, Michigan State University, East Lansing, Michigan, USA

<sup>9</sup>Center for Molecular Medicine and Genetics, Wayne State University, Detroit, Michigan, USA

<sup>10</sup>Philips Innovation Campus, Philips India Ltd., Bengaluru, India.

### Abstract

**Purpose:** To present the feasibility of performing quantitative susceptibility mapping (QSM) in the human fetus to evaluate the oxygenation ( $S_vO_2$ ) of cerebral venous blood *in-vivo*.

---

\*Corresponding authors: **Jaladhar Neelavalli, PhD**, Department of Radiology, Wayne State University School of Medicine, 4201 St. Antoine, Detroit, Michigan 48201, USA, Fax: +1 (313)745-9182, jneelava@med.wayne.edu, Roberto Romero, MD, D.Med.Sci., Perinatology Research Branch, NICHD/NIH/DHHS, Hutzell Women's Hospital, 3990 John R, 4 Brush, Detroit, Michigan 48201, USA, Phone: +1 (313)993-2700, Fax: +1 (313)993-2694, prbchiefstaff@med.wayne.edu.

Guarantor:

The scientific guarantor of this publication is Dr. Jaladhar Neelavalli.

Conflict of interest:

The authors of this manuscript declare no relationships with any companies, whose products or services may be related to the subject matter of the article.

Statistics and biometry:

No complex statistical methods were necessary for this paper.

Informed consent:

Written informed consent was obtained from all subjects (patients) in this study.

Ethical approval:

Institutional Review Board approval was obtained.

**Material and methods:** Susceptibility weighted imaging (SWI) data was acquired from healthy pregnant subjects (n=21, median=31.3weeks, IQR=8.8weeks). The susceptibility maps were generated from the SWI-phase images using a modified QSM processing pipeline, optimized for fetal applications. The processing pipeline is as follows: (1) mild high-pass filtering followed by quadratic fitting of the phase images to eliminate background phase variations; (2) manual creation of a fetal brain mask that includes the superior sagittal sinus (SSS); and (3) inverse filtering of the resultant masked phase images using a truncated k-space approach with geometric constraint. Further, the magnetic susceptibility,  $\chi_v$  and corresponding putative  $S_vO_2$  of the SSS were quantified from the generated susceptibility maps. Systematic error in the measured  $S_vO_2$  due to the modified pipeline was also studied through simulations.

**Results:** Simulations showed that the systematic error in  $S_vO_2$  when using a mask that includes a minimum of 5 voxels around the SSS and 5 slices remains <3% for different orientations of the vessel relative to the main magnetic field. The average  $\chi_v$  in the SSS quantified across all gestations was  $0.42\pm 0.03$  ppm. Based on  $\chi_v$ , the average putative  $S_vO_2$  in the SSS across all fetuses was  $67\%\pm 7\%$ , which is in good agreement with published studies.

**Conclusion:** This *in-vivo* study demonstrates the feasibility of using QSM in the human fetal brain to estimate  $\chi_v$  and  $S_vO_2$ .

## Keywords

magnetic resonance imaging; brain; second trimester

## 1. Introduction

Adequate oxygen supply to the fetus is an essential component of its normal growth and development [1]. Obstruction of this supply may lead to acute or chronic fetal hypoxia. This can be one of the major consequences of a compromised placental function, resulting from increased placental vascular resistance, preeclampsia, or an inflammatory condition [2-4]. An inadequate fetal response to hypoxia could render the fetal brain susceptible to injury [5, 6]. Indeed, chronic hypoxia is known to be a predictor of abnormal neurodevelopment and cognitive disabilities [7]. Therefore, the fetal cerebral blood oxygenation status could be an important physiological parameter in identifying fetuses at risk of brain injury. It is also an important quantity in understanding oxygen metabolism in the developing fetal brain in healthy homeostatic conditions.

Magnetic resonance imaging (MRI) is playing an increasingly important role in fetal diagnostic care. The ability to measure physiologic parameters, e.g., tissue metabolic status using MR spectroscopy (MRS) [8], volumetric blood perfusion using phase-contrast MRI [9], or blood oxygenation status using inherent tissue properties [10], has made MRI an important tool in quantitative fetal evaluation. MRS has the ability to detect and quantify the concentration of metabolites such as lactate, which is a downstream measure of tissue hypoxia [8]. Nevertheless, the ability to measure blood oxygen saturation would provide a direct measure of tissue hypoxia. Recent quantitative MRI-based works have used either the transverse relaxation rate property, T2, of blood [11] or the paramagnetic nature of deoxy-hemoglobin (dHb) with MR-susceptometry [10, 12] to measure blood oxygenation status *in-*

*in vivo* in the human fetus. Although the former method was successfully applied in the major vessels of the heart in third-trimester fetuses [11], it is susceptible to radiofrequency (RF) field inhomogeneities and is also associated with a high specific absorption rate (SAR), especially when imaging at 3.0T [13]. On the other hand, MR-susceptometry measures the magnetic susceptibility ( $\chi$ ) of blood that, in turn, is related to the amount of dHb present. It uses the phase signal from a spoiled gradient-echo (GRE) MRI sequence for performing this measurement, which is associated with a low SAR, even at 3.0T [14]. This method was recently applied in second- and third-trimester human fetuses to evaluate blood oxygenation ( $S_vO_2$ ) in the superior sagittal sinus (SSS) [10]. One of the challenges of the model-based susceptibility method, however, is that it uses only the intravascular phase and assumes that the vessel has no/minimal curvature with a circular cross-section, which is not true in all cases. Furthermore, it requires knowledge of the orientation of the vessel relative to the main magnetic field, which can be difficult to ascertain in the presence of vessel curvature.

Quantitative susceptibility mapping (QSM), on the other hand, uses both the intravascular and extravascular phase to estimate the  $\chi$  on a pixel-by-pixel basis. QSM is independent of the orientation and the shape/size of the structure of interest. Due to its ability to provide a direct measurement of the underlying spatial distribution of  $\chi$  across different tissues [15], it has been used to measure  $S_vO_2$  in the cerebral veins [16] and to detect hemorrhages or micro-bleeds [17]. QSM has also been used to diagnose hypoxic events and evaluate treatment efficacy in adults, children, and neonates [15, 18-20] [21, 22]. Although QSM holds tremendous potential to quantify blood  $S_vO_2$  non-invasively, it has not been translated to fetal imaging applications yet.

Hence, the goal of this study is to evaluate an optimized QSM processing pipeline for the quantification of the susceptibility of the fetal cerebral vessels. We also report the first application of QSM to quantify the putative fetal cerebral  $S_vO_2$ . Given that fetal structures are small and that the surrounding environment is unique compared to adult imaging, the modified QSM processing pipeline was first evaluated using a digital phantom for possible systematic errors in quantifying  $\chi_v$  and putative  $S_vO_2$ .

## 2. Material and Methods

### 2.1 Theory of QSM

Phase ( $\varphi(r)$ ) data provides a direct measure of the field perturbation,  $\Delta B(r)$  within a tissue relative to its immediate background. They are related by:

$$\varphi(r) = \gamma \cdot \Delta B(r) \cdot TE \quad (1)$$

where  $\gamma$  is the gyromagnetic ratio, and TE is the echo time. For biological materials with  $\chi \ll 1$ , spatial susceptibility distribution and the corresponding  $\Delta B(r)$  in the magnetizing field  $B_0$  can be related as follows [23]:

$$\Delta B(r) = FT^{-1} \left[ FT[\Delta\chi(r)] \cdot \frac{1}{3} - \frac{k_z^2}{k_x^2 + k_y^2 + k_z^2} \right] \cdot B_0 \quad (2)$$

where  $\chi(r)$  is the magnetic susceptibility distribution, FT is Fourier Transform and  $k_x$ ,  $k_y$ , and  $k_z$  are the coordinates in the spatial frequency domain, commonly referred to as k-space. Using Eqs. 1 and 2, the measured  $\varphi(r)$  in a tissue and the underlying  $\chi(r)$  property are related as:

$$\varphi(r) = \gamma \cdot FT^{-1} \left[ FT[\Delta\chi(r)] \cdot \frac{1}{3} - \frac{k_z^2}{k_x^2 + k_y^2 + k_z^2} \right] \cdot B_0 \cdot TE \quad (3)$$

Thanks to the paramagnetic nature of dHb, the  $\chi$  of venous blood is related to its oxygenation state via Eq.4 [24]:

$$\Delta\chi_v = \Delta\chi_{do} \cdot (1 - S_v O_2) \cdot Hct \quad (4)$$

where  $\chi_{do}$  represents the magnetic susceptibility difference between fully deoxygenated and fully oxygenated blood and  $Hct$  is the fractional hematocrit.

Re-writing Eq.3 for  $\chi(r)$ :

$$\Delta\chi(r) = FT^{-1} \left( FT \left( \frac{\Delta\varphi(r)}{\gamma \cdot B_0 \cdot TE} \right) \cdot \frac{1}{\frac{1}{3} - \frac{k_z^2}{k_x^2 + k_y^2 + k_z^2}} \right) \quad (5)$$

Eq.5 is the basis of the QSM approach that has been widely used to quantify *in-vivo* blood oxygenation [16, 25-29].

## 2.2 Patient Recruitment

Twenty-one women in their second (n=5) and third trimester (n=16) of pregnancy, who received routine obstetrical care at Hutzel Women's Hospital, Detroit, Michigan, EISA, were non-consecutively recruited in this study. The median and inter-quartile range (IQR) of gestational age (GA) of the fetuses included were 31.3 weeks and 8.8 weeks, respectively. MRI scanning was approved by the local Institutional Review Board (IRB) and was compliant with HIPAA regulations. Participants with a singleton, uncomplicated pregnancy with normal ultrasound examinations [10] and reporting no contraindications for MRI were eligible. Written informed consent was obtained before the MRI scan. Fetal SWI data was collected as part of a large study for which the total scan time was limited to 60 minutes.

### 2.3 Magnetic Resonance Imaging

Fetal MRI was carried out on a 3.0T Verio system (Siemens Healthineers) using a six-channel body-flex array coil, along with a spine coil. A fully flow-compensated 2D-/3D-SWI sequence was used to acquire fetal images [12]. The sequence parameters used are given in Table-1. In all subject scans, T2-HASTE and SWI data (either 2D-SWI or 3D-SWI or both) were acquired multiple times whenever fetal motion was encountered. SWI data were always acquired axial to the fetal brain.

### 2.4 Fetal QSM Pipeline and data analysis

Fetal SWI data were first reviewed for general quality, fetal motion, and other artifacts as well as for proper visualization of the SSS in both magnitude and phase in a series of minimum 5 consecutive images or over 15mm or 17.5mm. Thereafter, of the 21 pregnant subjects imaged with 2D-SWI (10), 3D-SWI (9), and both 2D- and 3D-SWI (2), their data were used for QSM processing.

QSM data were generated using the following steps (see Figure-1):

- 1) The raw phase data was corrected for the global phase offset by forcing the center phase of k-space to zero.
- 2) The phase of each image was then subjected to a background field removal method that included the application of homodyne high pass filtering (16×16), followed by a polynomial fitting for remnant low-spatial frequency phase removal.
- 3) A 3D brain mask was manually extracted from the filtered phase images, ensuring that it included the SSS.
- 4) The resultant phase data was then used as an input to the iterative, geometry constraint-based thresholded k-space division algorithm [16, 25] to generate QSM. This algorithm takes into account the slab orientation: hence, the orientation of the vein in 3 dimensions, relative to the  $B_0$  axis.
- 5) QSM images containing the SSS were zoomed twice using a nearest neighbor interpolation approach and a free hand region-of-interest (ROI) was drawn inside the SSS. The ROI contained a minimum of 10 voxels.
- 6) The mean and SD of the  $\chi_v$  distribution inside the SSS were measured from at least two central consecutive slices.
- 7) To enable comparison to previously published works,  $\chi_{do} = 4 * \pi * 0.27\text{ppm}$  [30, 31] and the reference  $Hct$  values [32] were used in Eq.3 to quantify the putative  $S_vO_2$  in the SSS.
- 8) When  $\chi_v$  (and  $S_vO_2$ ) measurements from multiple SWI volumes were available in a given fetus, the respective values were averaged.
- 9) The mean and standard error of  $\chi_v$  and  $S_vO_2$  were obtained across all fetuses.

The mean  $S_vO_2$  values obtained were compared to the results from previously published works [10, 12]. Furthermore, for each fetal SWI volume where a QSM analysis was performed, the conventional MR-susceptometry method was also applied to obtain  $S_vO_{2,s}$  as described by Neelavalli et al. [10, 12]. QSM-based and susceptometry-based oximetry values were compared using Bland-Altman as a measure of self-consistency in the quantified oxygenation value. A generalized linear model was also used to correlate the two methods. The statistical significance level was set at  $p < 0.05$ .

## 2.5 Simulations

The spatial extent of phase information in all 3 directions around the structure of interest is the primary parameter that influences the accuracy of susceptibility values in QSM. Hence, a simulation study using a digital brain phantom [12] was carried out to assess the systematic variability and predict the percentage error in the measured  $\chi_v$  ( $\delta \chi_v$ ) and the absolute error in fractional  $S_vO_2$  ( $\delta S_vO_2$ ) as a function of the mask region around the cross-section of the SSS and as a function of the number of slices (3-7 based on the acquired *in-vivo* data). Simulations were repeated for 5 different relative orientations of the brain with respect to the  $B_0$ :  $0^\circ$ ,  $\pm 30^\circ$  and  $\pm 60^\circ$ , to account for the variable fetal orientation *in-utero*.

The 3D digital brain phantom used is similar to the one described by Neelavalli et al., [12]. The susceptibility values used for the different tissues are listed in Table-2. The brain phantom was first set inside a  $1024 \times 1024 \times 1024$  matrix corresponding to an isotropic resolution of  $0.2 \text{ mm}^3$  and phase was simulated from this susceptibility matrix using the Fourier-based field perturbation estimation method [27]. The data was then condensed using Fourier cropping to obtain  $256 \times 256 \times 256$  matrix with a resolution of  $0.8 \times 0.8 \times 3 \text{ mm}^3$ , the same voxel size as that of the *in-vivo* data.

The in-plane mask size around the cross-section of the SSS was varied by factors of 2, 3, 4, 5, and 6 times the SSS diameter (i.e. x2, x3, x4, x5, and x6, respectively) (Figure-2). SSS diameter was determined by drawing a circle that exactly encompassed the SSS and then taking its diameter. Circular masks of increasing size (multiples of the vessel diameter) were then generated by fixing one boundary of the circle at the posterior aspect of the SSS and increasing their size in the anterior aspect as shown in Figure-2. This one sided region growth was to avoid the fetal skull and the immediate regions outside the fetal head, which often had unfaithful phase due to large susceptibility differences. An additional 5 voxels between the vessel boundary and the mask boundary on the posterior aspect of the vessel were ensured. This was carried out for 5 consecutive slices. The masks were asymmetric to accommodate the fact that the extra-vascular SSS phase is predominantly visible in the immediate brain parenchyma anterior to the vessel. In the posterior aspect of the vessel, phase is not measurable due to the very short  $T2^*$  of the cranium. Hence, the extent of the mask was limited to 5 voxels in the posterior aspect of the vessel. All the simulations were done using 5 slices.

In addition, the influence of the number of slices was evaluated by varying the slices containing the vessel, along the long-axis of the vessel, from 3-7 (with an increment of one) for the QSM processing. This was assessed at in-plane mask sizes of x2 (smallest) and x6

(largest).  $\delta \chi_v$  and  $\delta S_vO_2$  were finally assessed with respect to the ground truth value of 0.45ppm and the corresponding  $S_vO_2$  of 70%, for each simulation.

### 3. Results

#### 3.2 Simulations

For different sizes of the mask,  $\delta \chi_v$  and  $\delta S_vO_2$  were less than 3% across all vessel- $B_0$  orientations (Figure-3). Error in both  $\delta \chi_v$  and  $\delta S_vO_2$  increased as the number of slices and the mask size decreased. The  $\delta S_vO_2$  remained less than 3% ( $\delta \chi_v$ : <3%) for 5 slices for both extreme masks (x2 and x6), whereas it escalated to 10% ( $\delta \chi_v$ : <11%) and 3% ( $\delta \chi_v$ : <5%) when slices reduced to 3 for smaller (x2) and larger (x6) masks, respectively (Figure-4). Hence, for fetal QSM processing, at least 5 consecutive slices were used in all cases.

#### 3.1 Fetal QSM

Multiple slices of susceptibility maps of the fetal brain are shown in Figure-5. The SSS was clearly visible along with evidence of the central sinus. The mean  $\chi_v$  and  $S_vO_2$  in the entire fetal cohort (n=21) was  $0.42 \pm 0.03$  ppm and  $67\% \pm 7\%$ , respectively. The average  $\chi_v$  and  $S_vO_2$  in second- (n=5) and third-trimester (n=16) fetuses were  $0.29 \pm 0.02$  ppm,  $75\% \pm 5\%$ ; and  $0.47 \pm 0.03$  ppm,  $65\% \pm 7\%$ , respectively.

QSM-based  $S_vO_2$  and the corresponding susceptometry based  $S_vO_{2,s}$  measures are shown in table-3. The Bland-Altman analysis of QSM vs. susceptometry based measures shows very small bias of 0.01% and all the points, except one, lie within the 2 standard deviation range (-4.3 to 4.3) (Figure-6). This ascertains a strong correlation between the QSM-based  $S_vO_2$  and the  $S_vO_{2,s}$  measurements ( $R^2=0.96$ ;  $p < 10^{-14}$ ) for the same volumes of the fetal brain.

### 4. Discussion

We demonstrated the feasibility of generating QSM data in human fetuses, which was then used to estimate putative  $S_vO_2$  in the SSS. The average  $S_vO_2$  obtained is in close agreement with the values found in the fetal literature [12, 33, 34]. A  $\chi_{do}$  value for adult blood (0.27ppm [25]) was used in estimating the  $S_vO_2$  so that comparison to previously published susceptometry literature could be performed. A recent work [35] has shown that for third-trimester fetuses the  $\chi_{do}$  value is 0.21ppm. If we use this value, the average  $S_vO_2$  value would drop to 55%. However, this baseline shift in  $S_vO_2$  will not affect the conclusion of our feasibility study.

The QSM pipeline was adopted from the general adult QSM processing with some modifications. In the adult brain, commonly the Brain Extraction Tool (BET) [36] is used to generate binary masks of the brain-only region. However, due to factors such as the arbitrary orientation of the fetal brain, susceptibility artifacts from the close proximity of the gas-filled intestine and pubic/lumbar spinal bone, and presence of high-intensity regions, e.g., the maternal bladder, using BET for brain extraction was not possible. To overcome this issue, we manual segmented out the fetal brain from the filtered phase images and excluded

any regions corrupted by major artifacts. The mask was chosen such that the phase information around the SSS was preserved. Since the SSS lies on the posterior edge of the fetal brain, it was challenging to obtain a large symmetric region around the vessel due to the artifacts coming from the maternal organs. Therefore, we used an asymmetric region around the SSS (see Figure-1). Results from simulations provided an indication of the systematic errors that could be expected in the QSM processing due to the limited number of voxels around the SSS and the number of slices covering the SSS. The external phase behavior for a vein decays at a rate of  $\frac{1}{(\text{radius})^2}$ . Hence, the most dominant phase information required to reconstruct the susceptibility maps is present in the pixels nearest to the vein boundary. This was confirmed when we observed that  $\delta S_v O_2$  in the SSS remains less than 3%, provided the mask size, in the plane of the cross-section of the vessel, is twice the size of the diameter of the vessel and the vessel is contained in 5 slices. Results from the simulation study affirmed the reliability of the optimized pipeline for the fetal QSM used in this work.

To remove the background phase, we used a  $16 \times 16$  homodyne filter, followed by a quadratic fitting for edge preservation. The high-pass filter causes some level of phase signal loss depending on the size of the object [23]. However, a  $16 \times 16$  homodyne filter with an in-plane matrix of  $448 \times 448$  and a resolution of 0.8mm is equivalent to a filter that will affect structures of 35 pixels (28mm) in size or greater. Therefore, irrespective of the vessel orientation, the use of a small filter of  $16 \times 16$  leads to minimal loss of local phase of the fetal SSS whose maximum diameter is 4mm to 8mm at term [37].

Fetal SWI sequence used in this study was flow-compensated in all the three directions and hence,  $S_v O_2$  estimation in SSS was not affected by the blood flow. The QSM-based  $S_v O_2$  was highly correlated with the  $S_v O_{2,s}$  measured from the same volumes. MR susceptometry method uses intravascular phase to estimate  $S_v O_{2,s}$  which is dependent on the curvature and orientation of the blood vessel. It assumes the blood vessel to be a long cylinder. Although the straight section of the SSS was chosen for susceptometry, error may be present in  $S_v O_{2,s}$  due to a small error in the vessel angle and non-circular cross-section of the SSS. Compared to MR susceptometer, QSM does not rely on orientation and geometry based assumptions. Nevertheless, we found no statistical difference between the two techniques, which ascertains our results of accurate phase measurement using cylindrical approximation and confirms the accuracy and reproducibility of QSM measurements.

While the focus of our paper is the application of QSM technique to fetal blood oximetry, we observe that in our small sample size, the measured  $S_v O_2$  values in the second trimester group are higher than that in the third trimester group. This is consistent with the trend that was reported recently [10] and with that seen in previous in-vivo studies, where the blood oxygenation (both pO<sub>2</sub> and SO<sub>2</sub>) in umbilical venous blood samples, was been found to decrease with advancing gestational age [38-40]. Furthermore, it is also known that the cerebral blood flow rate to the human fetal brain increases from second to third trimester [41]. Taken together, the flow and oxygen saturation changes may be towards accommodating the increased metabolic demand that is seen during the third trimester.



There are some shortcomings in this study. First, the mask generation using manual intervention is time-consuming. We created a mask of all the slices containing the SSS in all the fetal data. An automated fetal BET would be very helpful in the future [42]. Second, for the simulations, we used a digital phantom that has features of the adult brain, which has less curvature in the SSS vessel than in the fetus. Nevertheless, we used the same spatial resolution as in our fetal data and chose slices from the curved region of the SSS in the simulations. This model provided a reasonable representation of the fetal brain. In addition, the cross section of SSS is an approximate triangle that might affect the precise formation of the mask sizes as a factor of SSS size. However, we tried to standardize our mask creation process by only moving the anterior point upwards to achieve different mask sizes. Third, we used longer TE in this study to achieve a good phase signal-to-noise ratio in SWI. A shorter TE could be more useful in QSM processing due to less  $T2^*$  signal loss and phase aliasing inside and at the boundaries of the veins. In addition, it could also help reduce the imaging time without sacrificing the phase SNR.

## 5. Conclusion

This study demonstrates the feasibility of using QSM in human fetuses. The putative  $S_vO_2$  of  $67\% \pm 7\%$  obtained from the  $\chi_v$  maps was in close agreement with previously published fetal literature.

## ACKNOWLEDGEMENTS

Dr. Romero has contributed to this work as part of his official duties as an employee of the United States Federal Government.

Funding:

This research was supported, in part, by the Perinatology Research Branch (PRB), Program for Perinatal Research and Obstetrics, Division of Intramural Research, Eunice Kennedy Shriver National Institute of Child Health and Human Development, National Institutes of Health, U.S. Department of Health and Human Services (NICHD/NIH/DHHS); in part, with Federal funds from NICHD/NIH/DHHS under Contract No. HHSN275201300006C; and an STTR grant from the NHLBI number 1R42HL112580-01A1.

## Abbreviations:

<b>Hct</b>	Hematocrit
$\chi_v$	Magnetic susceptibility
$\chi_{do}$	Magnetic susceptibility difference between fully oxygenated and deoxygenated fetal blood
$S_vO_2$	Venous oxygen saturation
<b>BET</b>	Brain Extraction Tool
<b>BW</b>	Bandwidth
<b>dHb</b>	Deoxyhemoglobin
<b>FA</b>	Flip angle

<b>FOV</b>	Field-of-view
<b>GA</b>	Gestational age
<b>GRE</b>	Gradient echo
<b>IQR</b>	Inter-quartile range
<b>IRB</b>	Institutional Review Board
<b>MRI</b>	Magnetic resonance imaging
<b>MRS</b>	MR spectroscopy
<b>QSM</b>	Quantitative susceptibility mapping
<b>RF</b>	Radiofrequency
<b>ROI</b>	Region of interest
<b>SAR</b>	Specific absorption rate
<b>SSS</b>	Superior sagittal sinus
<b>SWI</b>	Susceptibility weighted imaging
<b>TE</b>	Echo time
<b>TH</b>	slice thickness
<b>TR</b>	Repetition time
<b>US</b>	Ultrasound

## 6. References:

- Schneider H (2011) Oxygenation of the placental–fetal unit in humans. *Resp Physiol Neurobi* 178(1):51–8.
- Gagnon R (2003) Placental insufficiency and its consequences. *Eur J Obstet Gynecol Reprod Biol*. 110:S99–S107. [PubMed: 12965097]
- Maberry MC, Ramin SM, Leveno KJ, Dax JS. (1996) Intrapartum asphyxia in pregnancies complicated by intra-amniotic infection. *Obstet Gynecol*. 76(3):351–4.
- Escobar J, Teramo K, Stefanovic V, et al. (2013) Amniotic fluid oxidative and nitrosative stress biomarkers correlate with fetal chronic hypoxia in diabetic pregnancies. *Neonatology*;103(3):193–8. [PubMed: 23295371]
- Low JA, Galbraith R, Muir D, Killen H, Pater E, Karchmar E. (1958) The relationship between perinatal hypoxia and newborn encephalopathy. *Am J Obstet Gynecol*. 152(3):256–60.
- Gunn AJ, Bennet L. (2009) Fetal hypoxia insults and patterns of brain injury: insights from animal models. *Clin Perinato* 36(3):579–93.
- Hall D Birth asphyxia and cerebral palsy. (1989) *BMJ* 299(6694):279. [PubMed: 2504405]
- Cetin I, Barberis B, Brusati V, et al. (2011) Lactate detection in the brain of growth-restricted fetuses with magnetic resonance spectroscopy. *Am J Obstet Gynecol* 205(4):350. e1-. e7. [PubMed: 21861968]
- Krishnamurthy U, Yadav BK, Jella PK, et al. (2017) Quantitative Flow Imaging in Human Umbilical Vessels In Utero Using Nongated 2D Phase Contrast MRI. *JMRI*

10. Yadav BK, Krishnamurthy U, Buch S, et al. (2018) Imaging putative foetal cerebral blood oxygenation using susceptibility weighted imaging (SWI). *Eur Radiol.* 1–7.
11. Zhu MY, Milligan N, Keating S, et al. (2016) The hemodynamics of late-onset intrauterine growth restriction by MRI. *Am J Obstet Gynecol* 214(3):367. e1-. e17. [PubMed: 26475425]
12. Neelavalli J, Jella PK, Krishnamurthy U, et al. (2014) Measuring venous blood oxygenation in fetal brain using susceptibility-weighted imaging. *JMRI* 39(4):998–1006. [PubMed: 24783243]
13. Stuber M, Botnar RM, Fischer SE, et al. (2002) Preliminary report on in vivo coronary MRA at 3 Tesla in humans. *Magn Reson Med* 48(3):425–9. [PubMed: 12210906]
14. Neelavalli J, Mody S, Yeo L, et al. (2014) MR venography of the fetal brain using susceptibility weighted imaging. *JMRI* 40(4):949–57. [PubMed: 24989457]
15. Haacke EM, Liu S, Buch S, Zheng W, Wu D, Ye Y. (2015) Quantitative susceptibility mapping: current status and future directions. *Magn Reson Med* 33(1):1–25.
16. Haacke E, Tang J, Neelavalli J, Cheng Y. (2010) Susceptibility mapping as a means to visualize veins and quantify oxygen saturation. *JMRI* 32(3):663–76. [PubMed: 20815065]
17. Liu T, Surapaneni K, Lou M, Cheng L, Spincemaille P, Wang Y. (2012) Cerebral microbleeds: burden assessment by using quantitative susceptibility mapping. *Radiology.* 262(1):269–78. [PubMed: 22056688]
18. Deistung A, Schweser F, Reichenbach JR. (2012) Overview of quantitative susceptibility mapping. *NMB* 30(4).
19. Liu C, Wei H, Gong N-J, Cronin M, Dibb R, Decker K. (2015) Quantitative susceptibility mapping: contrast mechanisms and clinical applications. *Tomography: a journal for imaging research.* 1(1):3.
20. Liu C, Li W, Tong KA, Yeom KW, Kuzminski S. (2015) Susceptibility-weighted imaging and quantitative susceptibility mapping in the brain. *JMRI* 42(1):23–41. [PubMed: 25270052]
21. Carpenter KL, Li W, Wei H, et al. (2016) Magnetic susceptibility of brain iron is associated with childhood spatial IQ. *NeuroImage* 132:167–74. [PubMed: 26899787]
22. Liu J, Xia S, Hanks R, et al. (2016) Susceptibility weighted imaging and mapping of micro-hemorrhages and major deep veins after traumatic brain injury. *J neurotrauma.* 33(1):10–21. [PubMed: 25789581]
23. Haacke EM, Reichenbach JR. (2014) *Susceptibility weighted imaging in MRI: basic concepts and clinical applications*: John Wiley & Sons;
24. Weisskoff RM, Kiihne S. (1992) MRI susceptometry: Image-based measurement of absolute susceptibility of MR contrast agents and human blood. *Magn Reson Med* 24(2):375–83. [PubMed: 1569876]
25. Tang J, Liu S, Neelavalli J, Cheng Y, Buch S, Haacke E. (2013) Improving susceptibility mapping using a threshold-based K-space/image domain iterative reconstruction approach. *Magn Reson Med* 69(5):1396–407. [PubMed: 22736331]
26. de Rochefort L, Brown R, Prince MR, Wang Y. (2008) Quantitative MR susceptibility mapping using piece-wise constant regularized inversion of the magnetic field. *Magn Reson Med* 60(4): 1003–9. [PubMed: 18816834]
27. Wharton S, Schäfer A, Bowtell R. (2010) Susceptibility mapping in the human brain using threshold-based k-space division. *Magn Reson Med* 63(5):1292–304. [PubMed: 20432300]
28. Schweser F, Deistung A, Lehr BW, Reichenbach JR. (2010) Differentiation between diamagnetic and paramagnetic cerebral lesions based on magnetic susceptibility mapping. *Med phys.* 37(10): 5165–78. [PubMed: 21089750]
29. Neelavalli J, Cheng Y, Haacke M, editors. (2005) Method for susceptibility calculation in multiple source object distribution with arbitrary susceptibilities: a preliminary report *Proc Intl Soc Magn Reson Med.*
30. Spees WM, Yablonskiy DA, Oswood MC, Ackerman JJ. (2001) Water proton MR properties of human blood at 1.5 Tesla: Magnetic susceptibility, T<sub>1</sub>, T<sub>2</sub>, T<sub>2</sub>\* 2, and non-Lorentzian signal behavior. *Magn Reson Med* 45(4):533–42. [PubMed: 11283978]
31. Jain V, Abdulmalik O, Propert KJ, Wehrli FW. (2012) Investigating the magnetic susceptibility properties of fresh human blood for noninvasive oxygen saturation quantification. *Magn Reson Med* 68(3):863–7. [PubMed: 22162033]

32. Boulot P, Cattaneo A, Taib J, et al. (1993) Hematologic values of fetal blood obtained by means of cordocentesis. *Fetal Diagn Ther.* 8(5):309–16. [PubMed: 8267865]
33. Chua S, Yeong S, Razvi K, Arulkumaran S. (1997) Fetal oxygen saturation during labour. *BJOG-Int J Obstet Gy.* 104(9):1080–3.
34. Dildy GA, Thorp JA, Yeast JD, Clark SL. (1996) The relationship between oxygen saturation and pH in umbilical blood: implications for intrapartum fetal oxygen saturation monitoring. *Am J Obstet Gynecol* 175(3 Pt 1):682–7. [PubMed: 8828434]
35. Portnoy S, Milligan N, Seed M, Sled JG, Macgowan CK. (2017) Human umbilical cord blood relaxation times and susceptibility at 3 T. *Magn Reson Med.*
36. Smith SM. (2002) Fast robust automated brain extraction. *Hum brain mapp.* 17(3):143–55. [PubMed: 12391568]
37. Pooh RK, Kurjak A. (2010) Fetal brain vascularity visualized by conventional 2D and 3D power doppler technology. *DSJUOG.* 4:249–58.
38. Soothill PW, Nicolaides KH, Rodeck CH, Campbell S. (1986) Effect of gestational age on fetal and intervillous blood gas and acid-base values in human pregnancy. *Fetal Diagn Ther.* 1(4):168–75.
39. Nicolaides K, Economides D, Soothill P. (1989) Blood gases, pH, and lactate in appropriate-and small-for-gestational-age fetuses. *Am J Obstet Gynecol.* 161(4):996–1001. [PubMed: 2801852]
40. Schröter B, Chaoui R, Glatzel E, Bollmann R. (1997) Normwertkurven für intrauterine fetale Blutgas-und Säure-Basen-Parameter im 2. und 3. Trimenon [Normal value curves for intrauterine fetal blood gas and acid-base parameters in the 2nd and 3rd trimester]. *Gynakol Geburtshilfliche Rundsch.* 37(3):130–5. [PubMed: 9483871]
41. Veille J-C, Hanson R, Tatum K. (1993) Longitudinal quantitation of middle cerebral artery blood flow in normal human fetuses. *Am J Obstet Gynecol* 169(6):1393–8. [PubMed: 8267034]
42. Habas PA, Kim K, Corbett-Detig JM, et al. (2010) A spatiotemporal atlas of MR intensity, tissue probability and shape of the fetal brain with application to segmentation. *NeuroImage.* 53(2):460–70. [PubMed: 20600970]

**Study subjects or cohorts overlap:**

The imaging data used in this manuscript has been used in part previously in an earlier manuscript (Yadav BK, et al., Imaging putative foetal cerebral blood oxygenation using susceptibility weighted imaging (SWI). *Eur Radiol.* 2017 Dec 15. PMID:29247352), which evaluated fetal blood oxygenation as a function of gestational age in a larger cohort. This manuscript, on the other hand, focuses on demonstrating the applicability of a novel technique in the human fetus for in-vivo blood oximetry and compares the results with those obtained using the standard model-dependent method. We find that the results affirm the applicability of both methods for in-vivo fetal blood susceptometry and oximetry.

**Methodology:**

- prospective
- experimental
- performed at one institution

**Key points:**

1. A modified quantitative susceptibility mapping (QSM) processing pipeline is tested and presented for the human fetus.
2. QSM is feasible in the human fetus for measuring magnetic susceptibility and oxygenation of venous blood *in-vivo*.
3. Blood magnetic susceptibility values from MR susceptometry and QSM agree with each other in the human fetus.

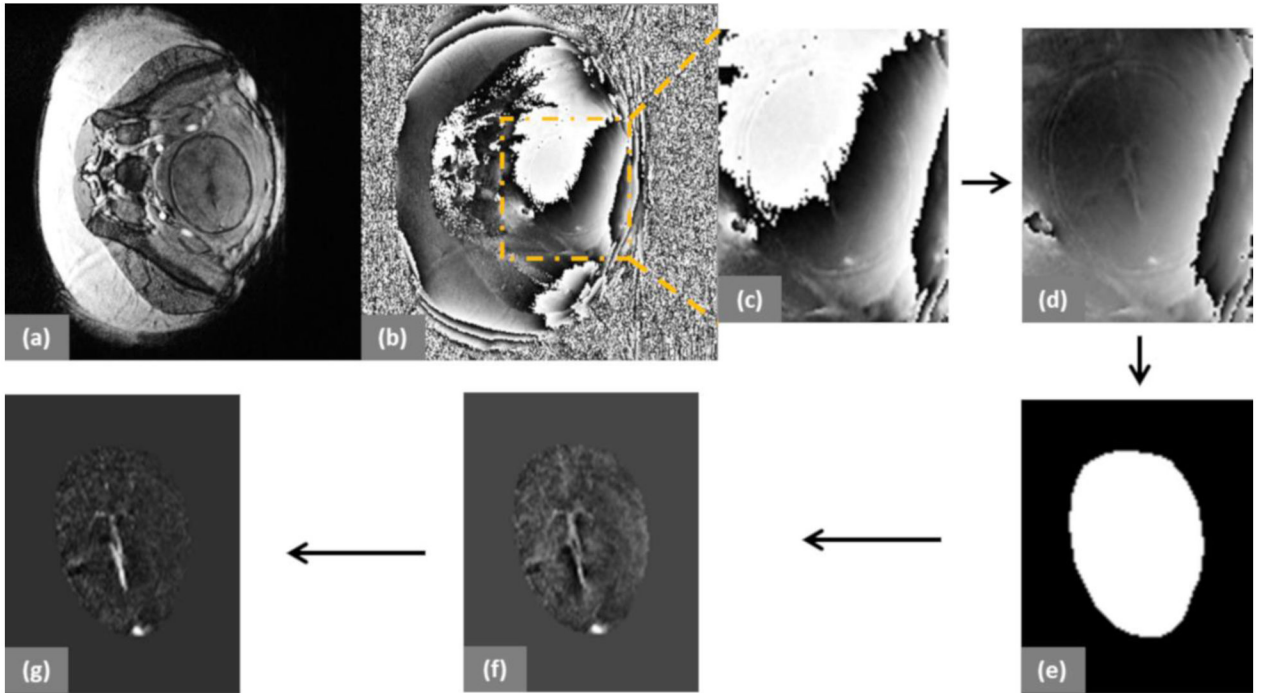


**Figure 1:**

Representative examples from a fetus at 31 3/7 weeks of gestation. (a) and (b) show the magnitude and phase images of a fetus inside the maternal abdomen. (c) Cropped raw phase image; (d) Phase-offset corrected phase image; (e) Binary mask of the fetal brain; (f) Phase image after background phase removal using a weak high-pass filter and quadratic fitting; and (g) QSM of the fetal brain.



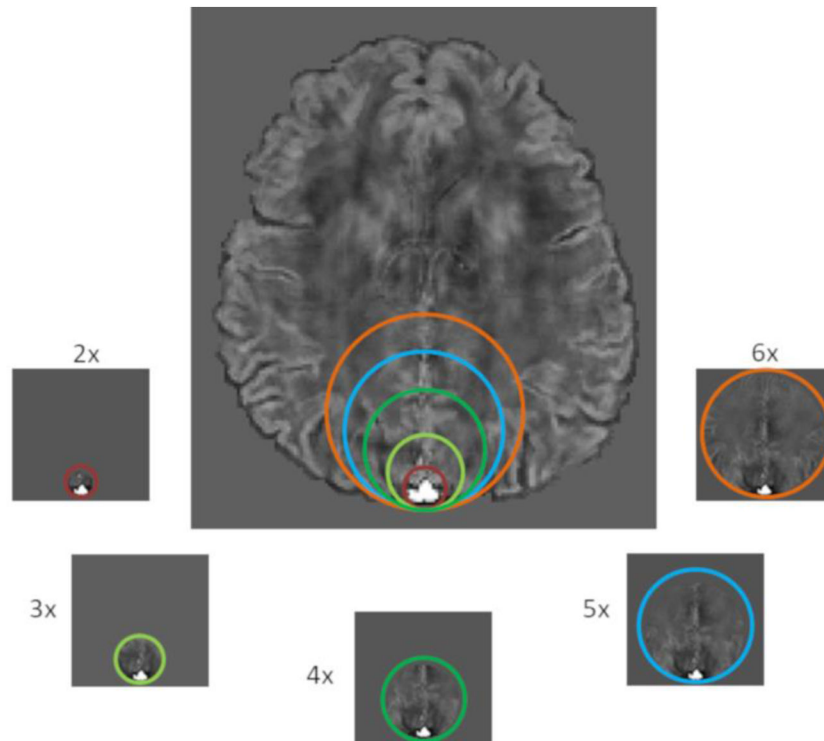


**Figure 2:**  
Mask generation: Different mask regions labeled x2, x3, x4, x5, and x6 as the sizes of SSS are created. The different sizes of the mask regions are highlighted with different colors.

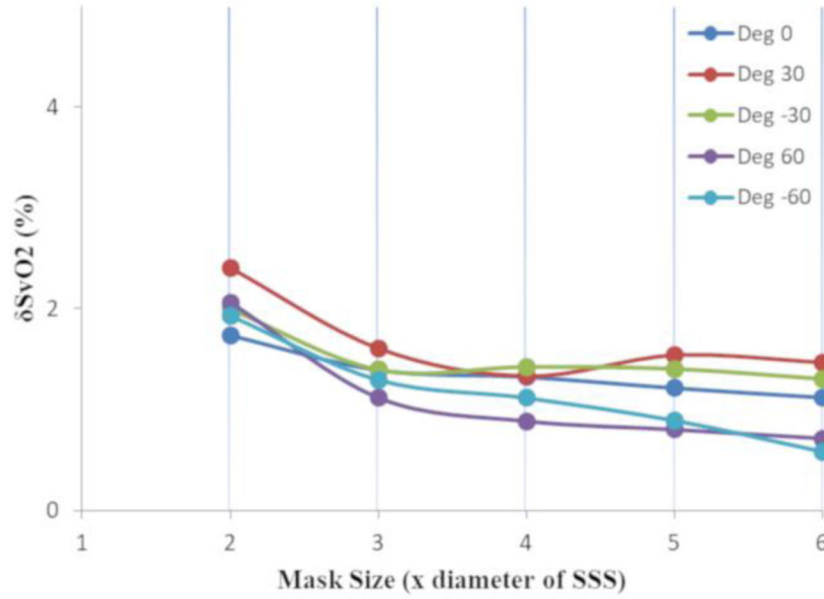


**Figure 3:** Relative  $\delta S_v O_2$  with respect to different mask sizes (relative to the diameters of the SSS) in the QSM of a digital brain is shown. The masks were asymmetric with fixed 5 voxels on the posterior side of the SSS and 5 slices containing the SSS. The results were obtained for various vessel orientations with respect to  $B_0$ . The error was found to be  $<3\%$ .

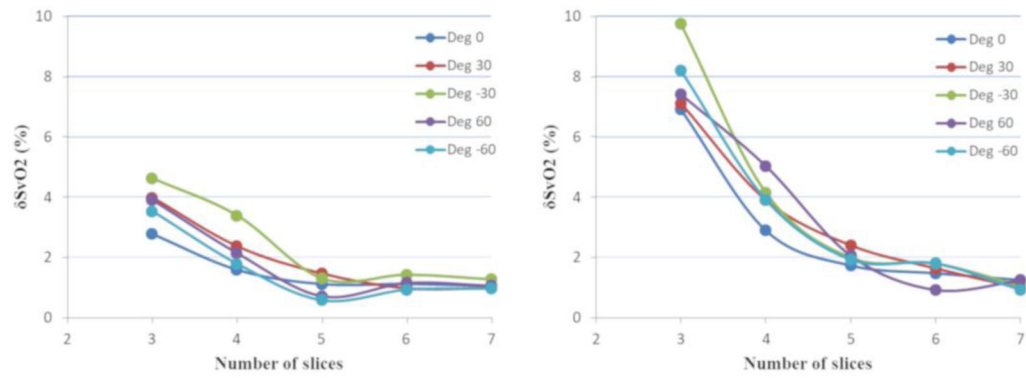


**Figure 4:** Relative  $\delta S_v O_2$  with respect to the different number of slices (3 to 7) used in the QSM of a digital brain phantom for (left) mask size 6 times larger than SSS and (right) mask size 2 times larger than SSS, are shown. The  $\delta S_v O_2$  decreases as the number of slices increases, which is  $<3\%$  for 5 slices for both the mask sizes and  $<5\%$  ( $\delta\chi_v: <6\%$ ) and  $<10\%$  ( $\delta\chi_v: <11\%$ ) for 3 slices for larger and smaller mask sizes, respectively.

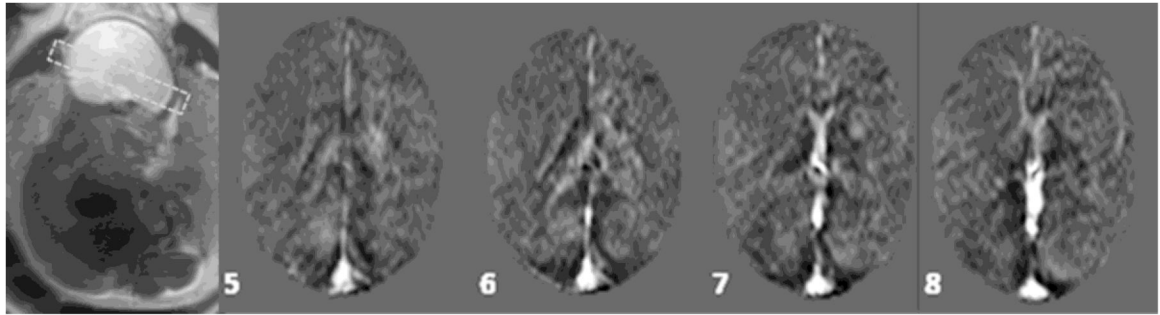


**Figure 5:**  
A collage of multiple slices (as numbered) showing the susceptibility maps of a fetal brain. Major vessels such as SSS, straight sinus, and transverse sinus can be seen along with small veins near the corpus callosum. GA: 29 weeks.

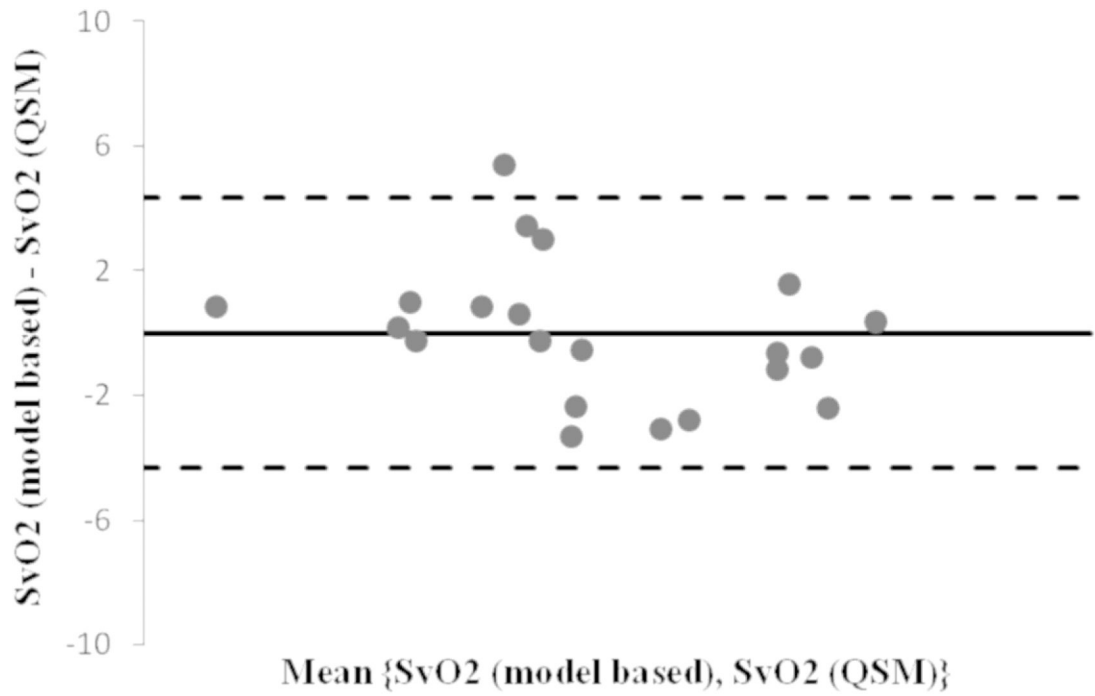


**Figure 6:**

The Bland-Altman plot (oxygenation difference vs. mean oxygenation of model based and QSM based methods) shows a small bias of 0.01% and all points, but one, lie within the 2\*standard deviation range. This ascertains a strong correlation between the two measurements  $R^2= 0.96$ ;  $p < 10^{-14}$ .

**Table 1:**

2D/3D MRI parameters of a fully flow-compensated SWI sequence. TR: repetition time, TE: echo time, FA: flip angle, TH: slice thickness, BW: bandwidth.

	TR (ms)	TE (ms)	FA (°)	Matrix	Resolution (mm <sup>2</sup> )	TH (mm)	# of Slices	BW (Hz/pixel)	Scan Time (sec)
<b>2D SWI</b>	280	15-18.7	32	448×168 - 448×175	0.78×1.56 - 0.85 × 1.7	3.5	10-11	199	22-24
<b>3D SWI</b>	23	13.5 - 17.3	10	448×175	0.78×1.56	3-3.5	16	219	22-24

**Table 2:**

Brain structures with corresponding magnetic susceptibility values in ppm units are shown. These values are used in the brain model for the simulation.

Brain Tissue	Magnetic Susceptibility (ppm)
Venous vessels	0.45
Gray matter	0.02
White matter	0
Red nucleus	0.13
Substantia nigra	0.16
Crus cerebri	0.03
Thalamus	0.01
Globus pallidus	0.18
Caudate nucleus	0.06
Putamen	0.09
Cerebrospinal fluid	0.014

**Table 3:**

The venous blood oxygenation values estimated using the QSM-based and MR susceptometry-based techniques.

Gestational Age (weeks)	Oxygenation using Susceptometry (%)	Oxygenation using QSM (%)
35.3	56.0±1.8	56.2±6.7
21	86.2±2.0	86.6±4.4
34.1	65.2±1.2	64.9±9.5
23.7	84.5±1.2	82.1±2.2
31.3	75.9±1.9	73.2±5.9
24	68.8±1.8	65.5±7.0
27.1	62.5±3.1	65.7±4.8
28.9	60.1±1.8	65.6±5.7
37.4	57.4±1.2	57.2±4.9
31.9	56.4±1.0	57.4±5.9
35.7	68.5±2.1	66.2±4.6
29	61.0±1.3	61.8±6.9
20.7	67.9±3.2	67.5±4.5
36.4	44.2±2.8	45.0±6.9
37	63.7±2.0	66.8±6.2
36.6	80.0±6.7	81.6±10.3
27.9	82.6±2.8	81.9±6.0
29	80.5±1.5	79.8±4.8
26.3	80.7±1.8	79.6±5.9
31.4	63.5±4.0	64.1±11.8
33.9	74.2±1.9	71.2±3.8